

Photocatalytic Degradation of Rhodamine 6G using TiO₂/WO₃ Bilayered Films Produced by Reactive Sputtering

L. C. Silva¹, B. Barrocas², M. E. Melo Jorge³ and S. Sérgio¹

¹CEFITEC, Departamento de Física, Faculdade de Ciências e Tecnologia da Universidade Nova de Lisboa, 2829-516 Caparica, Portugal

²Departamento de Química e Bioquímica, Faculdade de Ciências, Universidade de Lisboa, Campo Grande C8, 1749-016 Lisboa, Portugal

³Centro de Química e Bioquímica, Faculdade de Ciências, Universidade de Lisboa, Campo Grande C8, 1749-016 Lisboa, Portugal

Keywords: Photocatalysis, Rhodamine 6G, Reactive Sputtering, Decolorization, Bilayered Films.

Abstract: TiO₂/WO₃ and WO₃/TiO₂ bilayered films were deposited onto glass substrates by DC reactive magnetron sputtering and their photocatalytic activity was evaluated on the decolorization of Rhodamine 6G (Rh6G) aqueous solutions. The structures, morphologies and optical properties of TiO₂ and WO₃ layers and also of the bilayered films were studied by X-ray diffraction, field emission scanning electron microscopy and UV-Vis spectroscopy. It was found that the bilayered films exhibit good adherence to the substrates and high mechanic stability. The structural characterization revealed that in both nanocomposites independently of the above layer, the main phase observed in the X-ray patterns corresponds to WO₃ and the optical properties are similar to the WO₃ layer. The photocatalytic efficiency of the nanocrystalline bilayered films was further compared with TiO₂ and WO₃ films also produced by sputtering and the results show that the higher photocatalytic activity was achieved by the bilayered film with WO₃ as the upper layer.

1 INTRODUCTION

In the past years, the pollution of the wastewaters with dyes is becoming a huge environmental problem due to the growing use of a variety of dyes in several industries, namely textile, paper, plastics and cosmetic. These industries discharge large amount of colour effluents, which are very toxic and consequently can lead to serious ecological problems (Roy Choudhury, 2014). Dyes normally have a synthetic origin and complex aromatic molecular structures, which are very stable and difficult to biodegrade. It is also known that wastewaters containing dyes are very difficult to treat, since they are molecules resistant to aerobic digestion and are stable to oxidizing agents. Adsorption and coagulation are common methodologies applied to treat dyes but always result in secondary pollution (Ozmen, 2007, Crini, 2008).

Hence, it is extremely urgent to develop ecologically clean and safe chemical technologies, materials and processes to solve those problems. In line with these objectives, the application of

alternative methods like the advanced oxidation processes (AOP), such as photocatalysis has received great attention in the last years. Advanced oxidation processes (AOP), characterized by the production of hydroxyl radicals (OH·) and superoxide anion (O²⁻), which are generated when a semiconductor catalyst absorbs radiation when it is in contact with water and oxygen are a promising technology, in which a broad range of organic dyes can be oxidized quickly and non-selectively (Yang, 1998, Das, 1999). Among several photocatalysts, TiO₂ was extensively studied due to its inertness, nontoxicity, strong oxidizing activity and chemical stability (Mills, 1997, Grätzel, 2001). Nevertheless TiO₂ presents two important drawbacks for a wide practical application, such as the small percentage of the solar radiation, which has the required energy to photogenerate electrons and holes and their high recombination rate (Diebold, 2003, Thompson, 2006). In order to effectively use the energy of sunlight several approaches have been used to develop suitable photocatalysts and basically two strategies have been proposed. One is to modify the

wide band gap of the photocatalysts (such as TiO₂, ZnS) by cation or anion doping and the other approach is producing heterojunctions between them and other semiconductors. In fact, the increase in the photocatalytic efficiency in these heterogeneous systems results from the suppression of the recombination of the photogenerated charge carriers which results from the directional transfer of the photogenerated charges between different types of semiconductor particles (Akhavan, 2010, Krishnamoorthy, 1998, Nova, 2000). Therefore, a proficient way to extend the absorbance of TiO₂ to visible light is the development of heterojunctions of different nano-semiconductors including Fe₂O₃/TiO₂, TiO₂/SnO₂, ZnO/TiO₂ and WO₃/TiO₂ (Lin, 2008, Marci, 2001, Keller, 2003, Akhavan, 2009). These studies evidence a synergetic photocatalytic effect for a suitable combination of the semiconductors.

Photocatalysts can either be used as powders in a slurry form or as supported films. The latter configuration is advantageous since solves important problems such as the need for separation/filtration steps, the problematic use in continuous flow systems and the particles aggregation (Fernandez-Ibanez, 2003). Investigations on heterogeneous photocatalysis have been oriented towards the photocatalyst immobilization in film form. Many techniques can be used to prepare catalytic material immobilized in film form (Kavan, 1995, Shaogui, 2004, Sánchez-Mora, 2004, Celik, 2006) such as, sol-gel method, chemical vapor deposition, sputtering and others. Among them sputtering method presents several advantages such as high deposition rates, films with high purity, high adherence, accurate control of the film thickness and a wide industrial applicability.

This work reports a study of the preparation and characterization of TiO₂/WO₃ and WO₃/TiO₂ and the photocatalytic activity evaluation under visible light irradiation using the Rh6G as a target contaminant. Rh6G dye is a complex molecule and is extensively used for coloring leather, paper, silk and wool, which should be treated before being extruded into the environment.

2 EXPERIMENTAL DETAILS

TiO₂/WO₃ and WO₃/TiO₂ (being WO₃ and TiO₂, the upper layer, respectively) bilayered films were deposited by DC-reactive magnetron sputtering on glass substrates in a custom made system. Prior to the deposition, the substrates were cleaned

successively in acetone, isopropanol and deionized water for 5 min each step and dried with nitrogen gas to remove any organic contamination. A turbomolecular pump was used to achieve a base pressure of 10⁻⁴ Pa (before introducing the gas mixture). Before the sputter-deposition step of the films, a movable shutter was interposed between the target and the substrates, and the target was pre-sputtered in Ar atmosphere for 5 min to clean the target surface. The target-to-substrate distance was kept constant at 100 mm. The gases in the system were 99.99% pure Ar and O₂ and the partial pressures of these gases were separately controlled by mass flow controllers. One reference sample of TiO₂ film was deposited on a glass substrate using a metallic titanium disc (99.99% purity) as sputtering target. The total pressure, P_T, was kept constant at 0.8 Pa and the partial pressure of oxygen was set at 0.08 Pa (10% of P_T). The sputtering power was 1000 W and the deposition time was 80 min. In the case of WO₃ film, the total pressure, P_T, was kept constant at 1.2 Pa and the partial pressure of oxygen was set at 0.6 Pa (50% of P_T). The sputtering power used was 350 W and the deposition time was 25 min. The TiO₂/WO₃ and WO₃/TiO₂ bilayered films were prepared using the same deposition conditions of the reference films.

The structural characterization of the films was carried out by X-ray diffraction (XRD) on a Philips Analytical PW 3050/60 X'Pert PRO ($\theta/2\theta$) equipped with X'Celerator detector and with automatic data acquisition (X'Pert Data Collector (v2.0b) software), using a monochromatized CuK α radiation as incident beam, 40 kV–30 mA. Diffractograms were obtained by continuous scanning in a 2θ -range of 10° to 90° with a 2θ -step size of 0.02° and a scan step time of 20 s.

The surface morphology and thickness of the films were examined by field-emission scanning electron microscope (FEG-SEM JEOL 7001F). In order to prevent charge build up during analysis a thin chromium film was coated on the films.

The optical properties of the films were measured with Shimadzu UV b - 2101PC UV/VIS spectrophotometer at room temperature within the wavelength range 300-900 nm.

The photocatalytic activity of the reference films (TiO₂ and WO₃), TiO₂/WO₃ and WO₃/TiO₂ bilayered films was evaluated by the photocatalytic decolorization of Rh6G aqueous solution at ambient temperature under visible light irradiation. The photodegradation experiments were carried out in a photoreactor refrigerated by water circulation. The reaction vessel with a capacity of 250 mL,

manufactured from borosilicate glass accommodates a cooled central quartz tube, in which a 450 W Hanovia medium-pressure mercury-vapour lamp with 0.37 W/cm² of watt density is placed to irradiate the dye solution. Of the total irradiated energy, 40-48% is in the ultraviolet range and 40-43% in the visible region of the electromagnetic spectrum. In order to ensure illumination by only visible light, a cut off filter was placed around the cold trap to completely eliminate any radiation with wavelength below 400 nm. A magnetic stirrer was used to guarantee the solution homogenization.

The catalytic photodegradation experiments were performed carried out using one film with 9.72 cm² geometric area immersed on 175 mL of 5 ppm Rh6G aqueous solution prepared with ultrapure water. Prior to irradiation, the solution was magnetically stirred in absence of irradiation (in dark) for 1 h to establish the adsorption/degradation equilibrium between Rh6G and the photocatalyst. For convenience of the reader this period was represented by -10 min on the graphic representations. After this 1 h period the lamp was turned on. During irradiation, the solutions were sampled at regular intervals and analysed by UV-vis spectroscopy. The absorption of the Rh6G solutions and the rate of decolorization were observed in terms of change in intensity at λ_{\max} of the dye (526 nm). The decolorization efficiency percentage (*DE*) % of the catalyst was determined using the equation:

$$DE(\%) = (C_0 - C) / C_0 \times 100 \quad (1)$$

In which, C_0 is the dye initial concentration ($t = 0$ min) and C is the dye concentration after photoirradiation, which can be estimated from the characteristic absorption maximum in UV-vis spectroscopy at 526 nm. The blank experiment (Rh6G photolysis) was conducted in the presence of irradiation without any photocatalyst.

The structural stability and surface morphology of the photocatalysts were analyzed by XRD and diffuse reflectance infrared fourier transform spectroscopy (DRIFTS) before and after the photodegradation experiments.

3 RESULTS AND DISCUSSION

The structural characterization revealed that the as-prepared TiO₂ and WO₃ films are amorphous or poorly crystallized. In order to allow the crystalline growth, the films were thermal annealed at 400°C in tubular furnace in air during 4h. The XRD patterns,

for the annealed TiO₂ and WO₃ films, are presented in Figure 1. For the TiO₂ film the XRD pattern shows relative sharp peaks indicating the coalescence of nanocrystalline anatase-phase TiO₂ and exhibits a preferred orientation along the (004) direction. In the case of the WO₃ film, the diffraction peaks were assigned to the monoclinic WO₃ phase, which gave the best fit. Nevertheless, triclinic, orthorhombic and monoclinic diffraction peaks almost overlap for many 2θ values, namely the (002), (020) and (200) reflections at 2θ around 23-24° and it is difficult to discriminate between these three phases. According to the phase diagram, the monoclinic and triclinic structures are the most common structures and coexist in WO₃ at temperatures lower than 500 °C, the orthorhombic phase between 330 and 740 °C and, finally, a tetragonal structure up to 1230 °C (Naidu, 1991). Moreover, previous studies show that the diffraction pattern features at 2θ around 23-24° can suggest a mixture of the orthorhombic and the monoclinic WO₃ phases (Marsen, 2007), but can also arise from preferred orientation or from the presence of crystallographic shear planes (Jimenez, 2003). Therefore, in this work for the developed WO₃ films it cannot be discarded the presence also of the triclinic and orthorhombic phases due to the aforementioned reasons.

The inset in Figure 1 shows the surface morphology of the annealed WO₃ film analysed by SEM. The image shows agglomerates of grains or particulates, with spherical shape and average sizes of 100–250 nm distributed over the substrate surface with a ‘blooming flower-like’ appearance and others with an elongated shape with an average length of 200–300 nm.

The XRD patterns of the TiO₂/WO₃ and WO₃/TiO₂ bilayers films are depicted in Figure 2. By the comparison of Figure 1 with Figure 2 it can be detected that the XRD patterns of the bilayered films exhibit a main phase attributed to the monoclinic WO₃ phase (also as the WO₃ reference film, the presence of the triclinic and orthorhombic phases cannot be discarded) and only a small evidence of the anatase TiO₂ is observed in both heterojunctions independently of the above layer.

The surface morphology of the bilayered films was investigated by SEM and the images are presented in Figure 3. From the analysis of the images it is observed that when the above layer is WO₃ the film morphology consist of agglomerates of nano-sized grains or particulates, distributed over the substrate surface with a ‘blooming flower-like’ appearance (see Figure 3a) and an average size of 300-500 nm.

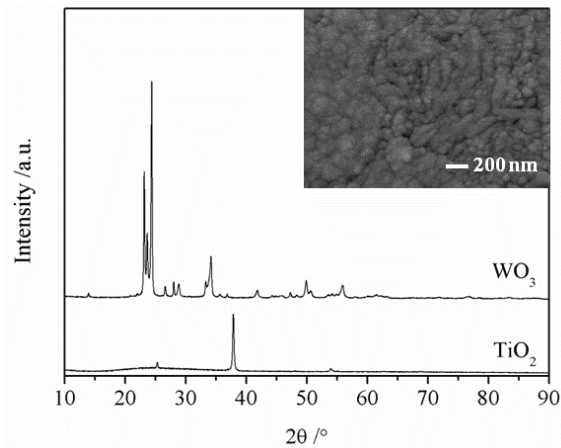


Figure 1: XRD patterns of the annealed TiO₂ and WO₃ films. The inset corresponds to a SEM image of the annealed WO₃ film surface.

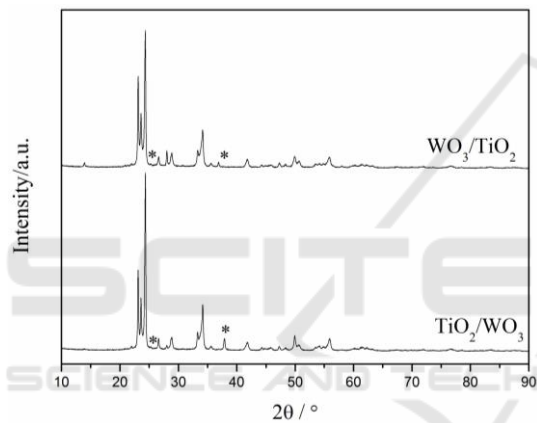


Figure 2: XRD patterns of the TiO₂/WO₃ and WO₃/TiO₂ bilayered films annealed at 400°C. *- corresponds to the anatase TiO₂ phase.

In the case of the nanocomposite film with the TiO₂ layer as the upper layer (see Figure 3b), the surface morphology is completely different although are visible agglomerates considerably smaller in comparison with the other nanocomposite with the WO₃ layer above. It is also noticeable a less dense surface with voids between the agglomerates.

The thicknesses were evaluated from FE-SEM cross-section images of the TiO₂ thin films, which are presented as inset of the corresponding films. The thicknesses of TiO₂ and WO₃ layers were approximately 990 nm and 2100 nm, respectively, in both bilayered films independently of the order of the layers.

Figure 4 shows the optical transmittance spectra of the TiO₂, WO₃ and of the bilayered films. The transmittance spectrum of the reference TiO₂ film shows the usual interference pattern in the range of

low absorption with a sharp fall of transmittance at the band edge around 350 nm. The annealed WO₃ film is light yellowish and nearly transparent. The band edge of WO₃ film is around 500 nm. The transmittance spectra of the TiO₂/WO₃ and WO₃/TiO₂ bilayered systems show almost similar nature as the WO₃ film. The average transmittance of TiO₂, WO₃, and TiO₂/WO₃ and WO₃/TiO₂ are 90%, 60%, and 58%, respectively.

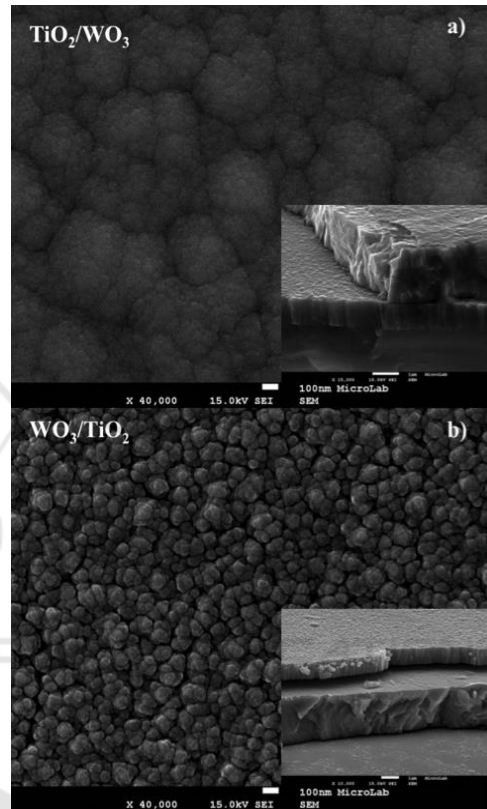


Figure 3: SEM images of the surface of the a) TiO₂/WO₃ and b) WO₃/TiO₂ nanocomposites films. The cross-section images of the nanocomposite films are presented as inset.

The optical band-gap of the TiO₂, WO₃ reference films were determined from the transmission spectra using Tauc's relation (Tauc, 1974), given as

$$\alpha E_{phot} = (E_{phot} - E_g)^m \quad (2)$$

in which, E_{phot} ($E_{phot} = 1239/\lambda$) is the excitation energy (in eV), with the wavelength λ in nanometers and m is a parameter accounting for the different band-gap transition modes, E_g is the optical energy band-gap and α is the absorption coefficient (in cm⁻¹), which is obtained near the absorption edge from the transmittance, T , using the equation

$$\alpha = d^{-1} \ln \left(\frac{1}{T} \right) \quad (3)$$

in which, d is the thickness of the film (Sério, 2011, Sério, 2012). In Eq. (2), the exponent m depends upon the type of optical transitions in the material. For indirect transitions, which is the case of TiO_2 and WO_3 films, the exponent takes the value (González-Borrero, 2010), $m = 2$.

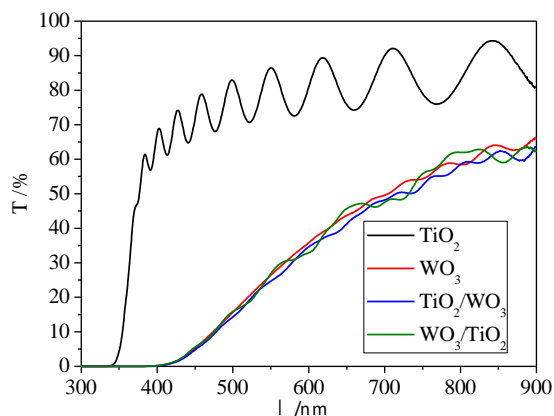


Figure 4: Optical transmittance spectra of the TiO_2 , WO_3 reference films and of TiO_2/WO_3 and WO_3/TiO_2 bilayered films.

The optical energy band gap was determined to be 3.33 eV for the TiO_2 reference film, whereas the optical energy band-gap for the WO_3 reference film comes out to be 1.97 eV. These values are in agreement with the published results for these type of oxides (Sério, 2011, Barrocas, 2013) and also evidence that the TiO_2 and WO_3 will be activated in the UV and visible range, respectively.

The photocatalytic activity of the bilayered and reference films was investigated under visible light irradiation on the decolorization of 5 ppm Rh6G solution for a period of 120 min. The Rh6G degradation was monitored by measuring the absorbance of the samples taken at regular intervals during a period of 120 min. The blank experiment without catalyst (photolysis) was also investigated. In Figure 5 is depicted a representative time dependent UV-vis spectra of Rh6G decolorization for the WO_3 catalyst. Similar time evolution decays were obtained for other catalysts.

From Figure 5, it is observed that the characteristic absorption peaks of Rh6G decrease with the increase of irradiation time. It is further observed that the Rh6G presents three characteristic absorption peaks: the peak at 247 nm is attributed to the benzene ring structure, the peak around 275 nm is related to the naphthalene ring structure and the third peak at 526 nm is the characteristic peak of Rh6G (Barrocas, 2013, Barrocas, 2014). The intensity of the peak at 526 nm dropped with the

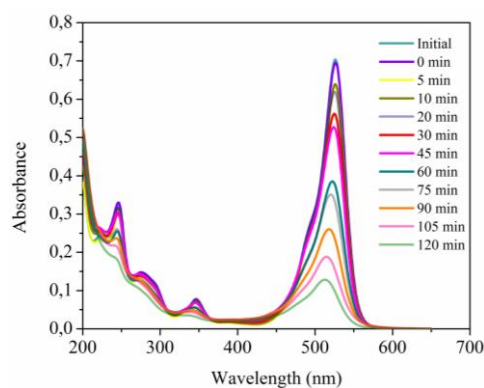


Figure 5: UV-vis absorption data for photocatalytic degradation of Rh6G solution upon irradiation with visible light, using WO_3 film as catalyst.

increase of irradiation time, which means that the chromophoric unsaturated conjugated bond in the dye molecule was gradually destroyed. The peak of benzene ring and naphthalene ring also decreased progressively with exposure time. These results indicate that the photocatalytic degradation not only destroys the conjugate system, but also partly decomposes the benzene and naphthalene rings in Rh6G molecule.

The rate of Rh6G decolorization was recorded considering the change in intensity of the absorption peak at 526 nm, during the 120 min of photoirradiation. Also the decay with time of the other Rh6G absorption bands is in accordance with complete degradation of the dye. The obtained results are present in Figure 6 for all the materials studied.

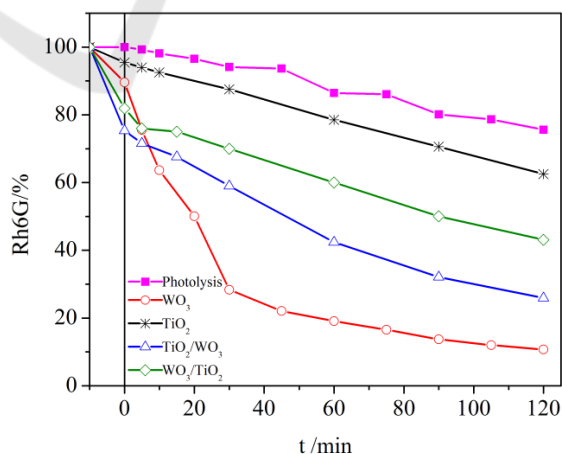


Figure 6: Rh6G degradation percentage evolution during the photocatalytic degradations of a 5 ppm aqueous solution using the reference films and the bilayered films as catalysts. The solid lines are guidelines for easy viewing.

As can be seen by Figure 6 analysis all the materials tested demonstrated to be catalytic in this photodegradation process. Without any catalyst, after 60 min of irradiation, less than 10% of Rh6G, were degraded. On the other hand, in the presence of WO₃, TiO₂, TiO₂/WO₃ and WO₃/TiO₂ after 60 min of irradiation approximately 80, 20, 65 and 45% of Rh6G, were degraded respectively. These results reveal that the WO₃ film exhibit the best photocatalytic performance, followed by the TiO₂/WO₃ bilayered film. However, the WO₃ film suffers of low mechanical stability, which isn't observed for the bilayered films independently of the upper layer. It is well known that the materials catalytic performance results from the balance of several factors such as the surface area, crystal structure, adsorption activity, band gap and so on. In this work and analyzing the band gap values obtained for these oxides the catalytic results point out that the lower band gap obtained for the WO₃ films and also for the bilayered films seems to be a preponderant factor on the films photocatalytic activity. It is further observed that in the case of the bilayered films, when the upper layer is WO₃ the photocatalytic activity is higher than the one observed for the other bilayered film when the upper layer is TiO₂. This difference in the catalytic activity may be attributed to the different surface morphology observed for these two types of bilayered films.

4 CONCLUSIONS

TiO₂/WO₃ and WO₃/TiO₂ bilayered films were deposited on glass substrates by DC-reactive magnetron sputtering. The bilayered films exhibit good adherence to the substrates and high mechanic stability. In both composites independently of the above layer, the main phase observed in the X-ray patterns corresponds to the WO₃. The bilayered films and in particular with WO₃ as the upper layer exhibit high catalytic performance for Rh6G degradation under visible irradiation which can be mainly attributed to the lower band gap in comparison with TiO₂ and also to the surface morphology. These findings are encouraging for future studies on the improvement of bilayered films photocatalytic efficiency and promote its practical application in environmental remediation using solar irradiation.

ACKNOWLEDGEMENTS

The authors acknowledge the financial support from FEDER, through Programa Operacional Factores de Competitividade – COMPETE and Fundação para a Ciência e a Tecnologia – FCT, for the projects UID/MULTI/00612/2013 and UID/FIS/00068/2013.

REFERENCES

- Akhavan, O., Azimirad, R., *Appl. Catal., A*, 369,77, 2009.
- Akhavan, O., *Appl. Surf. Sci.*, 257, 1724, 2010.
- Barrocas, B., Monteiro, O. C., Melo Jorge, M. E., Sério, S., *Appl. Surf. Sci.*, 264, 111–116, 2013.
- Barrocas, B., Sério, S., Rovisco, A., Melo Jorge, M.E., *J. Phys. Chem. C*, 118, 590–597, 2014.
- Celik, E., Yildiz, A. Y., Ak Azem, N. F., Tanoglu, M., Toparli, M., Emrullahoglu, O.F., Ozdemir, I., *Mater. Sci. Eng., B*, 129, 193, 2006.
- Crini, G., Badot, P. M. *Progress in polymer science*, 33(4), 399-447, 2008.
- Das, S., Kamat, P.V., Padmaja, S., Au, V., Madison, S. A., *J. Chem. Soc., Perkins Trans.*, 2, 1219-1224, 1999.
- Diebold, U., *Surf. Sci. Rep.*, 578, 48, 53–229, 2003.
- Fernandez-Ibanez, P., Blanco, J., Malato, S., de las Nieves, F.J., *Water Res.*, 37, 3180–3188, 2003.
- González-Borrero, P. P., Sato, F., Medina, A. N., Baesso, M. L., Bento, A. C., Baldissera, G., Persson, C., Niklasson, G. A., Granqvist, C. G., Ferreira da Silva, A., *Appl. Phys. Lett.*, 96, 061909, 2010.
- Grätzel, M., *Nature*, 414, 338, 2001.
- Jimenez, I., Arbiol, J., Dezanneau, G., Cornet, A., Morante, J. R., *Sens. Actuators, B*, 93, 475, 2003.
- Kavan, L., Grätzel, M., *Electrochim. Acta*, 40, 643, 1995.
- Keller, V., Bernhardt, P., Garin, F., *J. Catal.*, 215, 129, 2003.
- Krishnamoorthy, S., Baker, J. P., Amiridis, M. D., *Catal. Today*, 40, 39, 1998.
- Lin, C. F., Wu, C. H., Onna, Z. N., *J. Hazard. Mater.*, 154, 1033, 2008.
- Marci, G., Augugliaro, V., López-Munoz, M. J., Martín, C., Palmisano, L., Rives, V., Schiavello, M., Tilleyand, R. J., Venezia, A. M., *J. Phys. Chem. B*, 105, 1033, 2001.
- Marsen, B., Cole, B., Miller, E. L., *Sol. Energy Mater. Sol. Cells*, 91, 1954, 2007.
- Mills, A., Hunte S. Le, *J. Photochem. Photobiol., A*, 108, 1, 1997.
- Naidu, S. V. N., Rao, P. R., *Phase Diagrams of Binary Tungsten Alloys*, Indian Institute of Metals, Calcutta, 1991.
- Nova, I., Lietti, L., Tronconi, E., Forzatti, P., *Catal. Today*, 60, 73, 2000.
- Ozmen, E. Y., Erdemir, S., Yilmaz, M., Bahadir, M., *Clean: Soil, Air, Water* 35, 612–616, 2007.
- Roy Choudhury, A.K., *Environmental Impacts of the Textile industry and Its Assessment Through Life*

- Cycle Assessment, in: Muthu, S.S. (ed.), Roadmap to Sustainable Textiles and Clothing : Environmental and Social Aspects of Textiles and Clothing Supply Chain, Springer, Singapore, pp. 1-39, 2014.
- Sánchez - Mora, E., Gómez - Barojas, E., Gracia-Jiménez, J. M., Silva- González, R., Pérez- Rodríguez, F., Phys. Status Solidi C, 1, S116, 2004.
- Sério, S., Melo Jorge, M. E., Maneira, M. J. P., Nunes, Y., Mater. Chem. Phys., 126, 73, 2011.
- Sério, S., Melo Jorge, M. E., Nunes, Y., Barradas, N.P., Alves, E., Munnik, F., Nuclear Instruments and Methods in Physics Research Section B: Beam Interactions with Materials and Atoms, B 273, 109, 2012.
- Shaogui, Y., Xie, Q., Xinyong, L., Yazhi, L., Shuo, C., Guohu, C., Phys. Chem. Chem. Phys., 6, 659, 2004.
- Tauc, J., Amorphous and Liquid Semiconductors, Plenum, London, 1974.
- Thompson, T. L., Yates, J. T., Chem. Rev. 576, 106, 4428-4453. 577, 2006.
- Yang, Y., Wyatt, D. T., Bahorsky, M., Textile Chem. Colorist 30, 27-35, 1998.

